Stretch-activated force-shedding, force recovery, and cytoskeletal remodeling in contractile fibroblasts

Ali Nekouzadeh[1], **Kenneth M. Pryse**[2], **Elliot L. Elson**[2], and **Guy M. Genin**[3]

[1]*Cardiac Bioelectricity & Arrhythmia Center, Department of Biomedical Engineering, Washington University in St. Louis, St. Louis, Missouri, USA*

[2]*Department of Biochemistry and Molecular Biophysics, Washington University School of Medicine, St. Louis, Missouri, USA*

[3]*Department of Mechanical, Aerospace, and Structural Engineering, Washington University School of Medicine, St. Louis, Missouri, USA*

Abstract

The stress fiber network within contractile fibroblasts structurally reinforces and provides tension, or "tone", to tissues such as those found in healing wounds. Stress fibers have previously been observed to polymerize in response to mechanical forces. We observed that, when stretched sufficiently, contractile fibroblasts diminished the mechanical tractions they exert on their environment through depolymerization of actin filaments then restored tissue tension and rebuilt actin stress fibers through staged Ca^{++}–dependent processes. These staged Ca^{++}–modulated contractions consisted of a rapid phase that ended less than a minute after stretching, a plateau of inactivity, and a final gradual phase that required several minutes to complete. Active contractile forces during recovery scaled with the degree of rebuilding of the actin cytoskeleton. This complementary action demonstrates a programmed regulatory mechanism that protects cells from excessive stretch through choreographed active mechanical and biochemical healing responses.

Introduction

Myofibroblasts are the mechanical engines that shrink wound surfaces and provide homeostatically-regulated tension, or "tone", to scar tissue (1–4). The contractile mechanism by which myofibroblasts apply tension to their environment involves interactions between actin and non–muscle myosin in the cell's network of stress fibers and the connection of these stress fibers to the extracellular matrix (ECM) (2,3,5,6). External mechanical stressing can initiate a remodeling process that gradually increases tissue tension (7–10). We observed that contractile fibroblasts, which we treat as models of myofibroblasts, exhibit a self-protective mechanism for releasing excessive mechanical stresses and then restoring tension rapidly. Tension recovery arises from changes to the passive resistance (stiffness) of the de- and re-polymerizing actin cytoskeleton and a Ca^{++}–modulated contraction that scales with cytoskeletal rebuilding.

Conflicts of Interest
The authors have no relationships that could inappropriately influence or bias this work.

The results lend a tissue-level explanation for observations of intracellular Ca^{++} release associated with disruption of cytoskeletal elements (11,29). Results suggest that the structure, mechanics, and biochemistry of myofibroblasts combine in an intricate choreography to enable stress release for protection of internal structures followed by rapid tissue tension recovery as the cell rebuilds and remodels its cytoskeleton.

Materials and Methods

We studied three-dimensional cultures of contractile fibroblasts in a reconstituted collagen ECM. These tissue constructs serve as environments for quantification of cellular mechanics *in vitro* (11–15). Mechanical tests performed on ring-shaped tissue constructs in several biochemical environments were stopped through fixation at prescribed time-points to allow imaging through staining.

Specimens were synthesized using procedures described elsewhere (13). Briefly, fibroblasts isolated from 11-day-old chick embryos were incubated in Dulbecco's modified Eagle's medium (DMEM) at 37°C and 5% CO2 for 7 days, split, then incubated in DMEM for another 7 days. Fibroblasts acquired contractile features associated with myofibroblasts, including stress fibers (16,17); we term these "contractile fibroblasts" as their specific relationship to myofibroblasts requires further study, Cultured cells (2.0×10^6 cells/ml) were mixed with DMEM and type I rat tail collagen (1 mg/ml), and the pH was brought to neutral using NaOH. 1 ml of cell suspension was poured into Teflon molds composed of two concentric cylinders: the outer cylinder hollow (14.9mm inner diameter), and the inner solid (9.5mm diameter). The final suspension was incubated at 37°C and 5% CO_2 for 3 days as cells compressed and remodeled the collagen. After the first hour of incubation, molds were filled with DMEM containing 3% fetal bovine serum (FBS). The ring-shaped samples were mounted on a force measurement apparatus (18,19) and kept in HEPES-buffered DMEM (pH 7.4) containing 3% FBS at 37°C.

Mechanical testing began with a preconditioning protocol: a 30% stretch at 0.7 %/s, a 5 minute hold, a shortening back to the initial specimen length (0.7%/s), and a relaxation period of 40 minutes. The isometric tissue tension necessary to maintain the specimen at its original length was monitored to ensure that viscoelastic effects subsided. The relaxation test protocol was a rapid, 20% stretch of the sample, followed by a hold of 30 minutes as the isometric tissue tension required to maintain the specimen at this new length was monitored. The stretch rate of ~800%/s was sufficiently fast to be considered stepwise for the purpose of deriving viscoelastic properties, but sufficiently slow to neglect wave propagation within specimens (20). This procedure could be repeated multiple times with nearly identical results (Figure 6).

Specimens were returned to their reference configurations for a final test to measure the viscoelastic response of the remodeled ECM. 0.5%–1% Triton X-100 was added to the organ baths to disrupt the cells, and isometric tissue tension was monitored for 40 minutes as the Triton X-100 took effect and viscoelastic relaxation subsided. The relaxation test protocol was then repeated. The ECM was stable in the presence of Triton X-100 at these dosages (e.g. 21): isometric tissue tension reached a plateau after dissolution of the cells. Rhodamine phalloidin staining showed complete depolymerization of the actin cytoskeleton and membrane staining with DiD Orange (Invitrogen, Inc.) showed little remaining cell membrane.

To study the actin cytoskeleton during these tests, some samples were fixed at different phases using 1% paraformaldehyde during relaxation tests and permeablized using 0.1% Triton X-100. F-actin was stained with rhodamine phalloidin and 230×230 µm areas were imaged using confocal microscopy (1024×1024 pixels, 8-bit resolution). F-actin density and prevalence of stress fibers were quantified for ten randomly-selected images at each of four time-points in

the relaxation response (A–D, Figure 1c). F-actin density was measured from a 10% thresholding of images. This threshold level was sufficiently high to remove the variable effects of out-of-focus stress fibers from outside the imaging plane, and sufficiently low to retain pixels at the fringes of stress fibers within the imaging plane.

Prevalence of stress fibers was quantified using standard techniques for characterizing microstructures through X-ray scattering (22). Two-dimensional Fourier transforms of images were radial band-pass filtered, retaining only frequency pairs in the white band in the inset of Figure 4. Thin actin filaments, having diameters of 7–10 nm, affected only background stain intensity; since a pixel size of 225 nm was chosen, only thick actin filament bundles and stress fibers affected the Fourier transforms. Fourier transforms of images containing more stress fibers have more power in higher frequencies than those of images containing fewer stress fibers. Mean power density of the filtered Fourier transform (Figure 3), normalized by the pre-test value (time-point A), provided a measure of the prevalence of filaments with dimensions within a prescribed range of widths (38, supplemental document).

To study effects of external Ca^{++} on mechanical behavior, some samples were stretched in organ baths containing DMEM with 1.8mM Ca^{++}, and others in DMEM in which the Ca^{++} had been chelated using 2mM EGTA. To study effects of internal stores of Ca^{++}, some specimens were treated with thapsigargin to release internal stores of Ca^{++} (23), and then with BAPTA AM to chelate the internal Ca^{++}. In other tests, the Rho kinase pathway was down-regulated with Y27632 or up-regulated with nocodazole; nocodazole disrupts microtubules, causing phosphorylation of myosin light chains (MLCs) by MLC kinase and thereby activating actinmyosin contraction within the stress fibers (29).

Results

Contractile fibroblasts in ring-shaped, three-dimensional, reconstituted tissue constructs exhibited a characteristic isometric response after rapid stretching (Figure 1): a rapid rise, rapid shedding, rapid active recovery, plateau, and gradual active recovery of tissue tension. Mechanically preconditioned tissue constructs showed this most clearly. By the recovery's end, cells restored tissue tension to a target isometric value that increased with stretch amplitude.

Cellular mechanical response was estimated by subtracting the ECM contribution (Figure 1b), deduced from a mechanical test performed on the tissue construct after extracting cells using Triton X-100, from the overall mechanical response of the tissue construct (Figure 1a). This subtraction provided a reasonable approximation because of the high cellular density: in tissue constructs with cell populations sufficiently dense to form a contiguous network of mechanically connected cells, the mechanical contributions of cells and ECM are roughly additive (14,25,26).

After the rapid loss of tissue tension, contractile fibroblasts exhibited two mechanical recovery mechanisms. First (BC, Figure 1c), the mechanical tractions exerted by cells exhibited a rapid active response (the "RAR"), beginning ~2 seconds after the sudden stretch and lasting for ~50 seconds. These time intervals were independent of all test conditions including stretch magnitude, and were rapid compared to the contraction observed in wound healing and tissue remodeling (27). Second (CD, Figure 1c), cellular tractions exhibited a gradual active response (GAR), beginning a few minutes after the RAR and lasting for about 20 minutes, a timescale associated with isometric cellular contraction in response to biochemical agents and growth factors (11,28). These mechanisms each accounted for about 50% of the recovery from the minimum level of tissue tension (B, Figure 1c) to the stretch-dependent target level (D, Figure

1c). Between the RAR and GAR most tissue constructs exhibited a plateau in their isometric tension.

Both mechanisms operated through the contractile apparatus in the actin filament systems and produced contractile forces that scaled with the degree of rebuilding of stress fibers (Figure 2 and Figure 3). The stress-induced remodeling process involved rebuilding and alignment of stress fibers into the direction of external stressing. Prior to testing (Figure 2, image corresponding to Figure 1c, point A), contractile fibroblasts and their actin stress fibers exhibited a circumferential alignment determined by the constraint on the ring-shaped tissue constructs during incubation. This preferred direction coincided with the direction of the applied external stressing. During the tissue tension relaxation after the application of a sudden stretch (Figure 2, image corresponding Figure 1c, point B), continuous networks of stress fibers became disrupted, leaving loosely connected islands of stress fibers in the contractile fibroblasts. In addition to this reduction in connectivity, fewer actin filaments were visible, indicating depolymerization of actin filaments in response to the stretch. After finishing the RAR (Figure 2, image corresponding to Figure 1c, point C), the actin cytoskeletons showed repolymerization of stress fibers. By the end of the GAR (Figure 2, image corresponding to Figure 1c, point D) stress fibers had returned and the actin cytoskeletons recovered their continuous, dense appearance.

These qualitative observations were quantified through image analysis. By the onset of the RAR (point B, Figure 1c), approximately half of the actin cytoskeleton depolymerized in response to the external stressing, as measured by the area fraction of rhodamine phalloidin stain in the image. During the RAR (BC), a fraction of the actin filaments repolymerized, and by the end of the GAR (point D), the actin cytoskeleton returned to approximately the same or a slightly higher density of F-actin. The fraction of F-actin scaled with the cellular contribution to tissue tension, as shown by the gray trend line in Figure 2 (the trend line is the cellular contractile force curve, from Figure 1c, scaled to match the final data point in Figure 2).

In both the RAR and GAR, Fourier-space analysis indicated that actin repolymerized in the form of stress fibers, with no measurable change in the prevalence of cortical actin. Examination of power spectra showed that stress fibers depolymerized in response to the rapid stretch, repolymerized in proportion to the cellular contractile force throughout the RAR and GAR, and returned to approximately their pre-loading level after the GAR (Figure 3). The density of stress fibers, like the quantity of F-actin, paralleled the cellular contractile force: the trend line in Figure 3 is again the cellular contractile force curve (Figure 1c) scaled to match the final data point in Figure 3. Stress fiber alignment could also be found from the power spectra (e.g., 28): spreading of the frequency spectra in Figure 3 in the vertical relative to the horizontal direction indicated preferential alignment of stress fibers in the direction of stretch at all time points. Alignment dropped slightly after the sudden stretch, then returned to the pre-stretch level or slightly higher after the GAR.

The RAR occurred only in response to rapid stretching (>800%/s), while the GAR occurred in response to all stretch rates tested (Figure 6). The RAR appeared in the overall isometric tissue tension response as a recovery that eliminated relaxation in tissue tension, bringing the curve to a plateau. When the same specimen, under the same initial conditions, was subsequently subjected to a less rapid stretch (10%/s), the RAR was eliminated (Figure 6b): the relaxation rate reduced, and, although roughness in the curve due to cellular contraction was evident, the RAR and its arresting of stress relaxation was eliminated (Figure 6 a and b, inset). In both cases, the GAR appeared as a mild increase in the isometric tissue tension evident at approximately 500 seconds post-stretch.

The RAR was not associated with any permanent changes to the tissue constructs. Specimen preconditioning did not affect the RAR. When the specimen tested in Figure 6 was reloaded a third time, following the protocol of the first test, the RAR was recovered (Figure 6c).

Contractile force shedding in these experiments occurred through disruption of the actin cytoskeleton (Figure 2 and Figures 3). Estimates of cellular contributions to the overall isometric response (Figure 1c) showed that cells shed contractile force more rapidly (<1 sec) than could be accounted for through passive viscoelastic relaxation of cells or ECM (14,19): remodeled tissue constructs and their components exhibit a continuous, uniform spectrum of relaxation timescales over the course of at least an hour, and passive relaxation thus results in logarithmic relaxation far slower than that observed (24). Additionally, passive viscoelasticity would predict a higher peak tissue tension in stepwise tests than in slower tests (Figure 6), but no such effect was observed.

Contraction in both the RAR and GAR was triggered by Ca^{++}. Removing Ca^{++} from the external medium using EGTA delayed the onset of the GAR and reduced the level of tissue tension recovery in the GAR by 40% (Student's *t*-test parameter $t(6)=2.76$, $p=0.033$), but had an insignificant effect on the level of tissue tension recovery in the RAR (Figure 4). Removing both internal and external Ca^{++} using EGTA, thapsigargin, and BAPTA AM eliminated all active tension recovery (Figure 5) and affected the passive viscoelastic response.

Actin-myosin contraction through the Rho kinase pathway, known to drive sustained contractions in myofibroblasts, appeared to be significant in both the RAR and GAR. Up-regulation and down-regulation of this pathway through treatment with nocodazole and Y27632 scaled the baseline, RAR, and GAR cellular contractile forces upwards and downwards, respectively (data not shown).

Discussion

Contractile fibroblasts responded to rapid length increases through (*i*) a rapid force increase, associated with elastic resistance; (*ii*) rapid tissue tension shedding, associated with both viscoelastic relaxation and actin cytoskeleton disruption; and (*iii*) rapid (RAR) and gradual (GAR) restoration of tissue tension, associated with rebuilding of the actin cytoskeleton. The RAR, a rapid response to disruption of actin stress fibers, acted within seconds of a sudden stretch and completed in under a minute; the GAR began a few minutes post-stretch and lasted more than 20 minutes. Both were accompanied by cytoskeletal structural changes. Increased baseline cellular force following the GAR was consistent with passive elastic resistance of the cells. However, active, choreographed structural and biochemical factors contributed to the distinct mechanisms underlying the RAR and GAR.

Rapid stretching initiated depolymerization of some stress fibers, diminishing active forces exerted by cells proportionately. Increased passive elastic force from elongation of the remaining cytoskeletal components compensated to some degree, with the result that the nadir in cellular force response (point B in Figure 1c) was close to the pre-stretch level. Active cellular force increased during the RAR and GAR in direct proportion to the stress fiber density (Figure 2 and Figure 3).

Mechanics of tissue constructs containing contractile fibroblasts has been studied through many other protocols including isometric variations of tissue tension (29,30), isotonic variations of tissue length (31,32), and cyclic and other mechanical conditionings (9,33–35). However existing theories cannot explain the RAR and GAR. Brown et al. (28) studied the isometric force response of tissue constructs following linear increments in tissue tension and termed the isometric force reduction following elongation (or isometric force recovery following shortening) 'tensional homeostasis.' These observations differ fundamentally from

the current results. First, 'tensional homeostasis' refers to a reduction in isometric force after stretching, but the RAR and GAR are active increases in response to stretching. Second, the RAR requires activation through rapid stretching of the tissue construct (Figure 6); Brown et al. did not explore such conditions. Third, the RAR and GAR counteract passive viscoelastic relaxation; 'tensional homeostasis' acts in parallel with passive viscoelastic relaxation.

The cellular contractile forces in the RAR and GAR result from interactions between nonmuscle myosin and actin stress fibers. MLC phosphorylation through the Rho kinase pathway is believed to be dominant for myofibroblast contraction in wound healing and tissue remodeling (3,6,32,36). However, elimination and addition of Ca^{++} in cells and extra-cellular medium showed both the RAR and GAR to be highly sensitive to Ca^{++} levels, indicating an important role for the calcium pathway via MLC kinase.

Our experiments motivate a mechanism for the RAR and GAR in which contractile forces within stress fibers are regulated and maintained through the Rho kinase pathway, but the regeneration of stress fibers is regulated independently through a Ca^{++}-dependent pathway: here, Ca^{++} affects cellular contractile force through modulation of stress fiber polymerization and organization, but not through modulation of the contractile forces exerted by individual stress fibers. Release of internal stores of Ca^{++} and transient elevation of Ca^{++} concentration are known to occur with rapid stretching of lung epithelial cells (37): cytoplasmic Ca^{++} concentration increases 3.5-fold following a rapid stretch, then returns to pre-stretch levels within 60 seconds, the approximate duration of the RAR. Our results suggest that this Ca^{++} release serves to activate a quick partial restoration of stress fibers and tissue tension during RAR. The actin cytoskeleton continues to rebuild gradually during the GAR and approaches or exceeds its prestretch stress fiber density as active cellular force is restored.

Why do contractile fibroblasts exhibit these active responses? Rapid, sustained straining of contractile fibroblasts occurs, for example, in injured tendons during and after a change of posture. Reduction in cell stiffness through disruption of stress fibers shields cells from high stresses in the same way that microcracks in brittle composites can shield defects (38). Cytoskeletal disruption may shield cell-cell adhesions, cell-matrix adhesions, and internal cellular components connected to the actin cytoskeleton from large stresses in the same way that sacrificial bonds absorb energy and preserve vital structures in bone (39). Thereafter, contractile fibroblasts initiate a quick partial restoration of tissue tension during the RAR, completed, following a window if inactivity, in the GAR.

Supplementary Material

Refer to Web version on PubMed Central for supplementary material.

Acknowledgements

References

1. Ross R, Benditt EP. Wound healing and collagen formation V. Quantitative electron microscope radioautographic observations of proline-H3 utilization by fibroblasts. J Cell Biol 1965;27(1):83–106. [PubMed: 5859922]
2. Hinz B, Gabbiani G. Mechanisms of force generation and transmission by myofibroblasts. Curr Opin Biotechnol 2003;14(5):538–546. [PubMed: 14580586]
3. Tomasek JJ, Gabbiani G, Hinz B, Chaponnier C, Brown RA. Myofibroblasts and mechano-regulation of connective tissue remodelling. Nat Rev Mol Cell Biol 2002;3(5):349–363. [PubMed: 11988769]

4. Gabbiani G. The role of contractile proteins in wound healing and fibrocontractive diseases. Methods Achiev Exp Pathol 1979;9:187–206. [PubMed: 763158]

5. Dugina V, Fontao L, Chaponnier C, Vasiliev J, Gabbiani G. Focal adhesion features during myofibroblastic differentiation are controlled by intracellular and extracellular factors. J Cell Sci 2001;114(Pt 18):3285–3296. [PubMed: 11591817]

6. Chrzanowska-Wodnicka M, Burridge K. Rho-stimulated contractility drives the formation of stress fibers and focal adhesions. J Cell Biol 1996;133(6):1403–1415. [PubMed: 8682874]

7. Costa KD, Hucker WJ, Yin FC. Buckling of actin stress fibers: a new wrinkle in the cytoskeletal tapestry. Cell Motil Cytoskeleton 2002;52(4):266–274. [PubMed: 12112140]

8. Iba T, Sumpio BE. Morphological response of human endothelial cells subjected to cyclic strain in vitro. Microvasc Res 1991;42(3):245–254. [PubMed: 1779881]

9. Wang JH, Goldschmidt-Clermont P, Yin FC. Contractility affects stress fiber remodeling and reorientation of endothelial cells subjected to cyclic mechanical stretching. Ann Biomed Eng 2000;28 (10):1165–1171. [PubMed: 11144977]

10. Deshpande VS, McMeeking RM, Evans AG. A bio-chemo-mechanical model for cell contractility. Proc Natl Acad Sci U S A 2006;103(38):14015–14020. [PubMed: 16959880]

11. Kolodney MS, Wysolmerski RB. Isometric contraction by fibroblasts and endothelial cells in tissue culture: a quantitative study. J Cell Biol 1992;117(1):73–82. [PubMed: 1556157]

12. Wakatsuki T, Elson EL. Reciprocal interactions between cells and extracellular matrix during remodeling of tissue constructs. Biophys Chem 2003;100(1–3):593–605. [PubMed: 12646393]

13. Wakatsuki T, Kolodney MS, Zahalak GI, Elson EL. Cell mechanics studied by a reconstituted model tissue. Biophys J 2000;79(5):2353–2368. [PubMed: 11053115]

14. Zahalak GI, Wagenseil JE, Wakatsuki T, Elson EL. A cell-based constitutive relation for bio-artificial tissues. Biophys J 2000;79(5):2369–2381. [PubMed: 11053116]

15. Griffith LG, Swartz MA. Capturing complex 3D tissue physiology in vitro. Nat Rev Mol Cell Biol 2006;7(3):211–224. [PubMed: 16496023]

16. Kreis TE, Birchmeier W. Stress fiber sarcomeres of fibroblasts are contractile. Cell 1980;22(2 Pt 2): 555–561. [PubMed: 6893813]

17. Serini G, Gabbiani G. Mechanisms of myofibroblast activity and phenotypic modulation. Exp Cell Res 1999;250(2):273–283. [PubMed: 10413583]

18. Nekouzadeh A, Pryse KM, Elson EL, Genin GM. A simplified approach to quasi-linear viscoelastic modeling. J Biomech 2007;40(14):3070–3078. [PubMed: 17499254]

19. Pryse KM, Nekouzadeh A, Genin GM, Elson EL, Zahalak GI. Incremental mechanics of collagen gels: new experiments and a new viscoelastic model. Ann Biomed Eng 2003;31(10):1287–1296. [PubMed: 14649502]

20. Nekouzadeh A, Genin GM, Bayly PV, Elson EL. Wave motion in relaxation-testing of nonlinear elastic media. Proc. R. Soc. A 2005;461:1599–1626.

21. Engvall E, Hessle H, Klier G. Molecular assembly, secretion, and matrix deposition of type VI collagen. J Cell Biol 1986;102(3):703–710. [PubMed: 3456350]

22. Guinier, A. Crystals, Imperfect Crystals, and Amorphous Bodies. New York: Dover; 1994. X-Ray Diffraction.

23. Thastrup O, Cullen PJ, Drobak BK, Hanley MR, Dawson AP. Thapsigargin, a tumor promoter, discharges intracellular Ca2+ stores by specific inhibition of the endoplasmic reticulum Ca2(+)-ATPase. Proc Natl Acad Sci U S A 1990;87(7):2466–2470. [PubMed: 2138778]

24. Marquez JP, Genin GM, Pryse KM, Elson EL. Cellular and matrix contributions to tissue construct stiffness increase with cellular concentration. Ann Biomed Eng 2006;34(9):1475–1482. [PubMed: 16874557]

25. Marquez JP, Genin GM, Zahalak GI, Elson EL. The relationship between cell and tissue strain in three-dimensional bio-artificial tissues. Biophys J 2005;88(2):778–789. [PubMed: 15596491]

26. Marquez JP, Genin GM, Zahalak GI, Elson EL. Thin bio-artificial tissues in plane stress: the relationship between cell and tissue strain, and an improved constitutive model. Biophys J 2005;88 (2):765–777. [PubMed: 15596492]

27. Shreiber DI, Barocas VH, Tranquillo RT. Temporal variations in cell migration and traction during fibroblast-mediated gel compaction. Biophys J 2003;84(6):4102–4114. [PubMed: 12770913]

28. Nobe H, Nobe K, Paul RJ. Fibroblast fiber contraction: role of C and Rho kinase in activation by thromboxane A2. Am J Physiol Cell Physiol 2003;285(6):C1411–C1419. [PubMed: 12904286]

29. Kolodney MS, Elson EL. Contraction due to microtubule disruption is associated with increased phosphorylation of myosin regulatory light chain. Proc Natl Acad Sci U S A 1995;92(22):10252–10256. [PubMed: 7479762]

30. Brown RA, Prajapati R, McGrouther DA, Yannas IV, Eastwood M. Tensional homeostasis in dermal fibroblasts: mechanical responses to mechanical loading in three-dimensional substrates. J Cell Physiol 1998;175(3):323–332. [PubMed: 9572477]

31. He Y, Grinnell F. Stress relaxation of fibroblasts activates a cyclic AMP signaling pathway. J Cell Biol 1994;126(2):457–464. [PubMed: 7518467]

32. Parizi M, Howard EW, Tomasek JJ. Regulation of LPA-promoted myofibroblast contraction: role of Rho, myosin light chain kinase, and myosin light chain phosphatase. Exp Cell Res 2000;254(2):210–220. [PubMed: 10640419]

33. Prajapati RT, Chavally-Mis B, Herbage D, Eastwood M, Brown RA. Mechanical loading regulates protease production by fibroblasts in three-dimensional collagen substrates. Wound Repair Regen 2000;8(3):226–237. [PubMed: 10886813]

34. Shirinsky VP, Antonov AS, Birukov KG, Sobolevsky AV, Romanov YA, Kabaeva NV, Antonova GN, Smirnov VN. Mechano-chemical control of human endothelium orientation and size. J Cell Biol 1989;109(1):331–339. [PubMed: 2545727]

35. Mott RE, Helmke BP. Mapping the dynamics of shear stress-induced structural changes in endothelial cells. Am J Physiol Cell Physiol 2007;293(5):C1616–C1626. [PubMed: 17855768]

36. Tomasek JJ, Vaughan MB, Kropp BP, Gabbiani G, Martin MD, Haaksma CJ, Hinz B. Contraction of myofibroblasts in granulation tissue is dependent on Rho/Rho kinase/myosin light chain phosphatase activity. Wound Repair Regen 2006;14(3):313–320. [PubMed: 16808810]

37. Wirtz HR, Dobbs LG. Calcium mobilization and exocytosis after one mechanical stretch of lung epithelial cells. Science 1990;250(4985):1266–1269. [PubMed: 2173861]

38. Genin GM, Hutchinson JW. Composite Laminates in Plane Stress: Constitutive Modelling and Stress Redistribution Due to Matrix Cracking. Journal of the American Ceramic Society 1997;80(5):1245–1255.

39. Thompson JB, Kindt JH, Drake B, Hansma HG, Morse DE, Hansma PK. Bone indentation recovery time correlates with bond reforming time. Nature 2001;414(6865):773–776. [PubMed: 11742405]
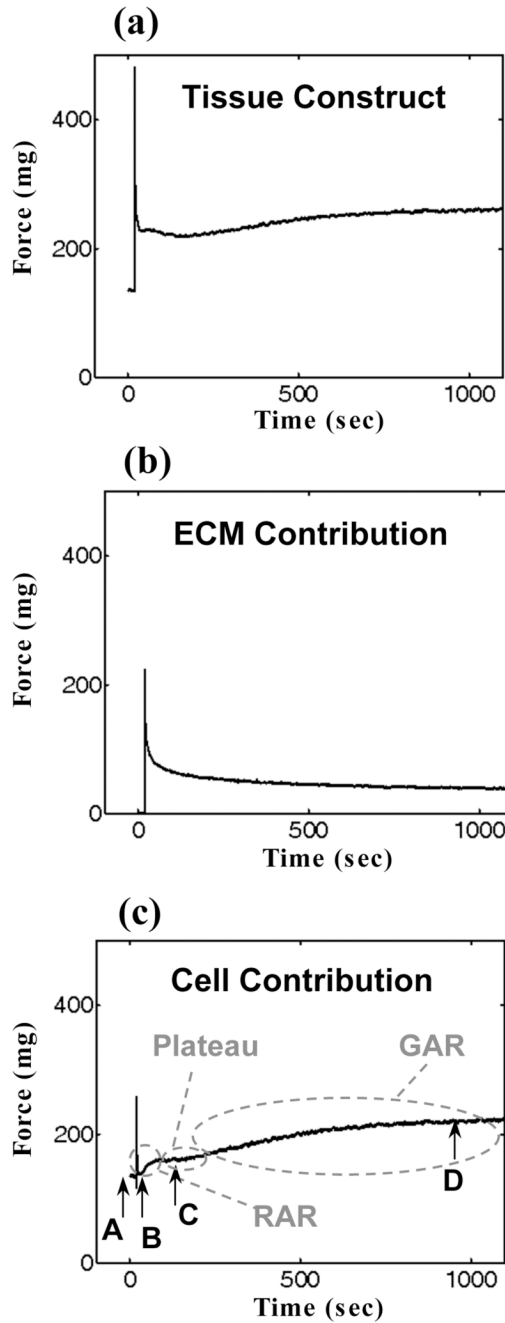
Figure 1. Mechanical responses of a tissue construct and its constituents to a rapid stretch
(**a**) Characteristic rapid rise, rapid shedding (~2 sec), rapid (RAR: ~50 sec) active recovery, plateau, and gradual (GAR: ~1000 sec) active recovery of tissue tension in a preconditioned tissue construct. (**b**) The extracellular matrix (ECM) contribution to overall tissue construct response, estimated by removing cells through treatment with Triton 100-X. The ECM response was entirely passive. (**c**) The cellular response, estimated by subtracting Figure 1b from Figure 1a.
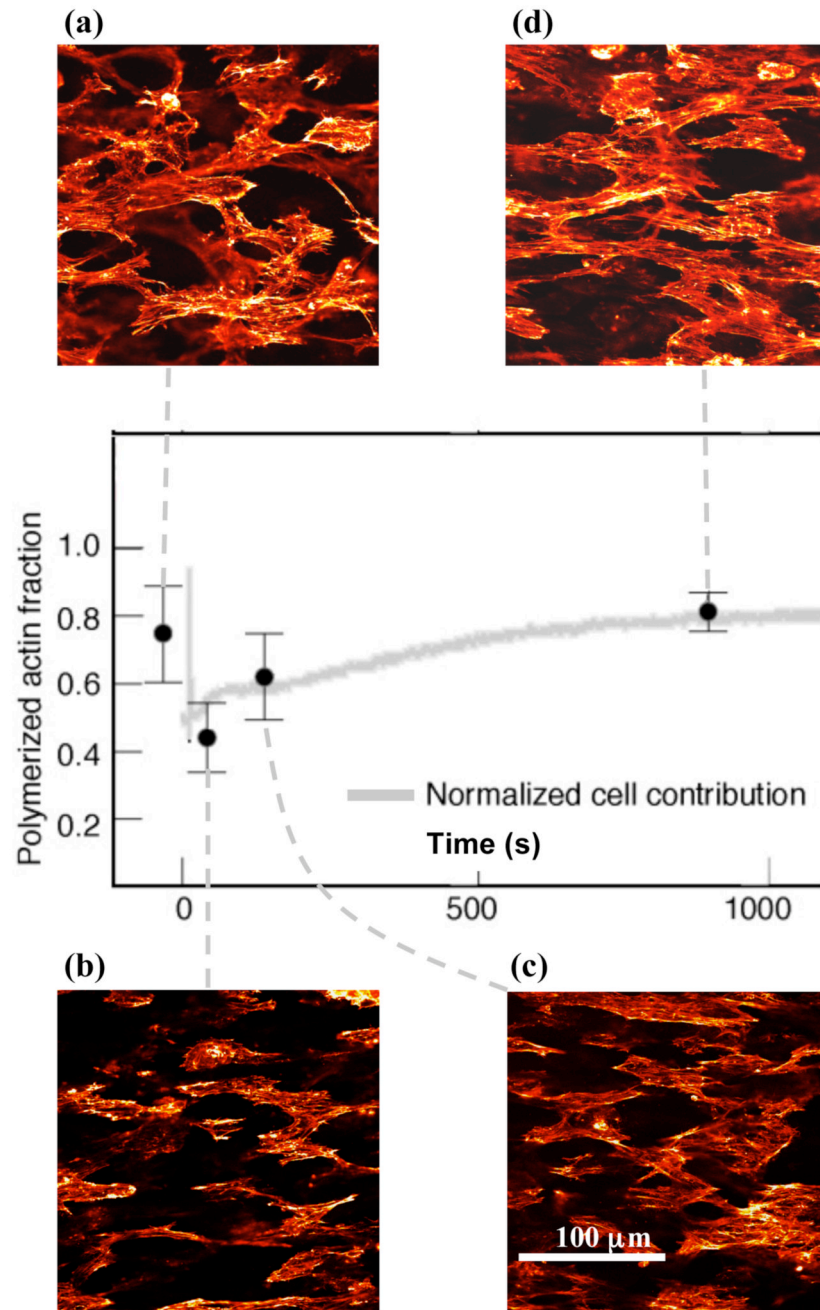
Figure 2. Breakdown and remodeling of the actin cytoskeleton in response to rapid external stressing quantified by the density of F-actin at four time points
(**a**) after preconditioning and before the relaxation test protocol, (**b**) at the end of the load-shedding following a step stretch (beginning of the RAR), (**c**) at the end of the RAR, and (**d**) at the end of the GAR. The graph shows the F-actin density calculated by integrating over a 10% black and white thresholding of images at each time-point. The trend-line is the cellular response curve from Figure 1c scaled to match the density at the end of the GAR. Error bars represent the range of data. The density of actin filaments scaled with the active cell force.
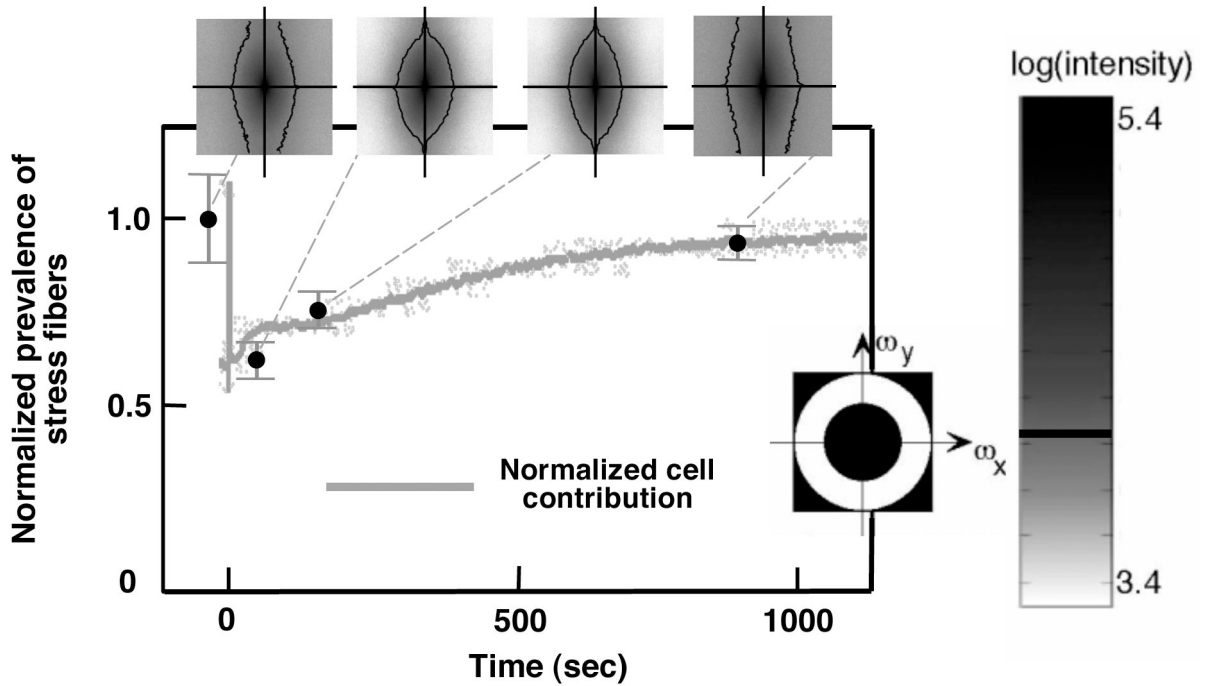
Figure 3. Regeneration of stress fibers correlated with the cellular force rise in both the RAR and GAR

The density of stress fibers at the four time points was calculated from the Fourier transforms of the images in Figure 2 (see supplementary document for details). The power spectra of the Fourier transforms of these images are pictured, with the vertical axes corresponding to frequencies ω_y in the direction perpendicular to stretch, and the horizontal axes corresponding to frequencies ω_x in the direction of stretch; darker colors correspond to higher amplitudes for the associated frequency pair (ω_x, ω_y). The prevalence of stress fibers was calculated by integrating over the white band in the band-pass filter illustrated in the inset; values were normalized by the pre-test value. The trend line is cell force curve from Figure 1c, scaled to match the stress fiber density at time D, near the end of the GAR. Error bars represent the range of data.
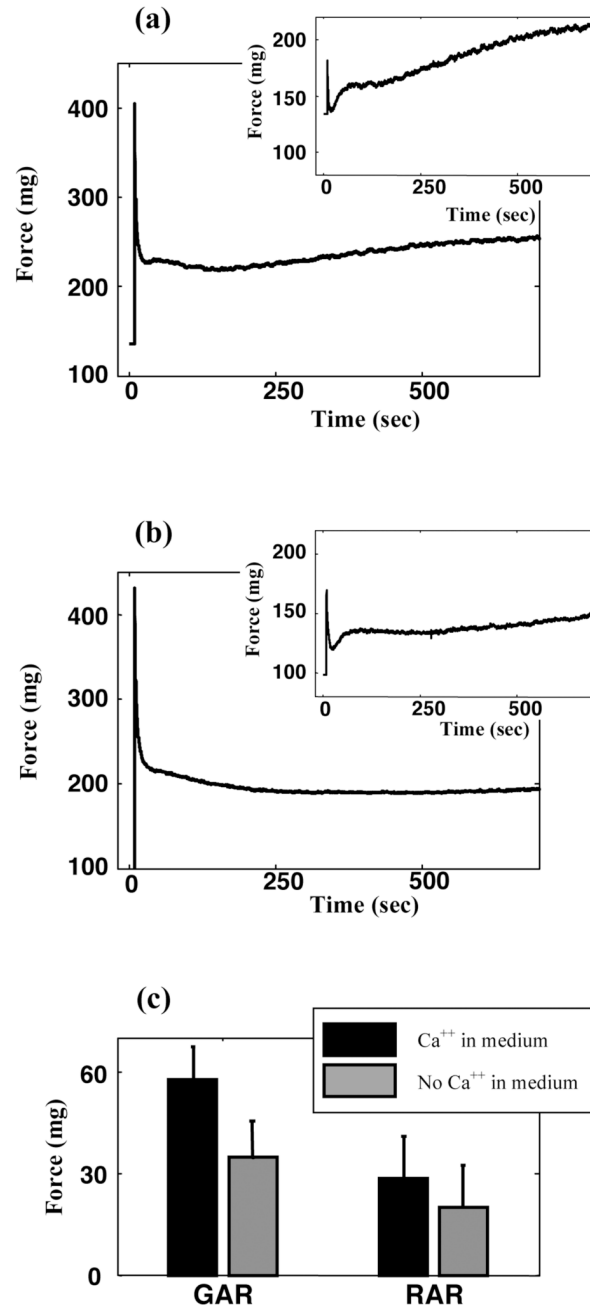
Figure 4. Effect of external calcium on the active responses of contractile fibroblasts
(**a**) Mechanical response of a tissue construct with 1.8mM Ca^{++} in the extracellular medium; inset shows the cellular contribution to this response, estimated as in Figure 1c. (**b**) Mechanical response of a tissue construct when extracellular calcium was chelated using 2mM EGTA; inset shows the cellular contribution. (**c**) Amplitudes of cellular force recovery in the GAR and RAR in specimens tested in medium containing with 1.8mM Ca^{++} (black), and in medium in which extracellular calcium was chelated using 2mM EGTA (gray). Error bars show the range of data from four specimens.
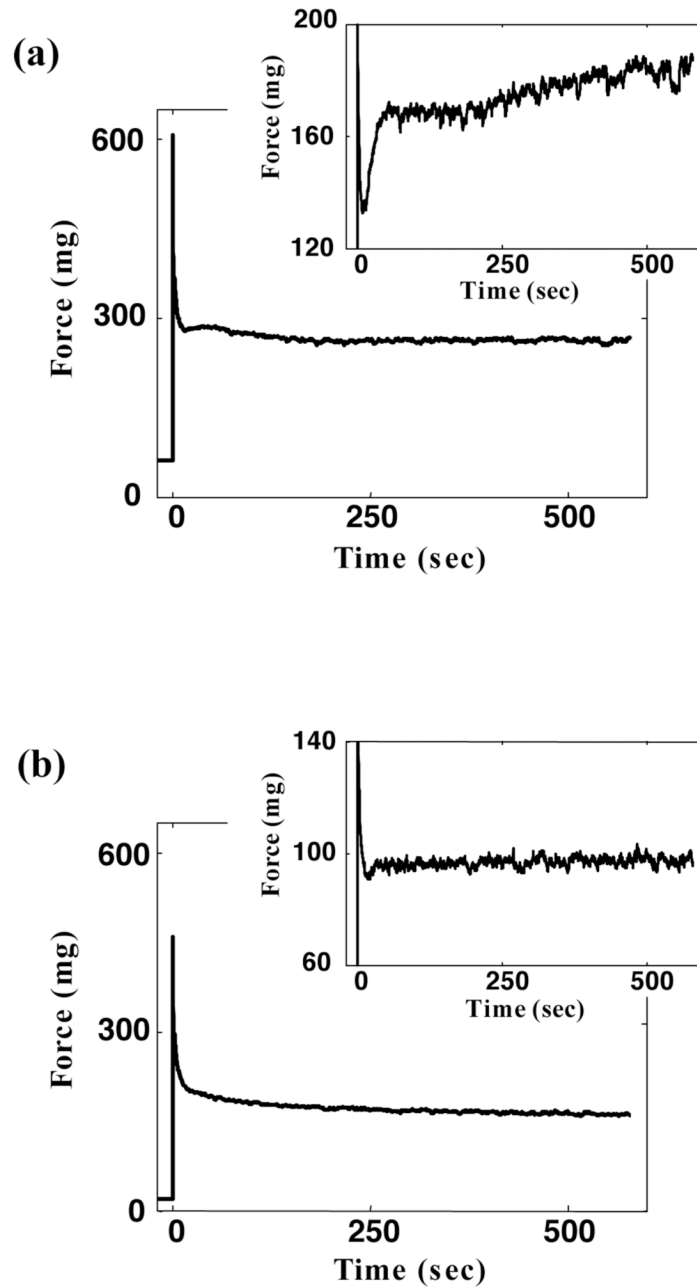
Figure 5. Combined effect of internal and external calcium on active responses of contractile fibroblasts
(**a**) Mechanical response of a tissue construct tested in a medium containing Ca^{++}. (**b**) Mechanical response of a tissue construct in which internal Ca^{++} was eliminated and Ca^{++} in the testing medium was chelated. Removal of Ca^{++} eliminates both the RAR and the GAR. Insets show the cellular contributions to these mechanical responses.
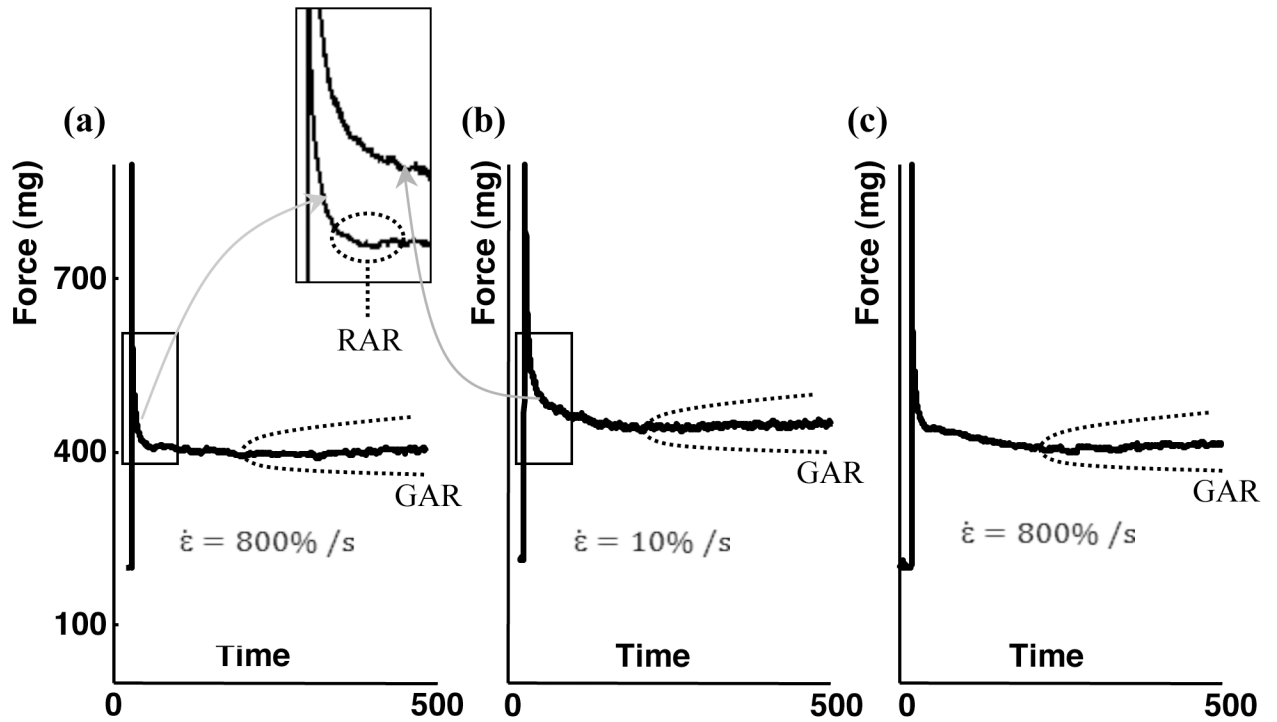
Figure 6. Effect of stretch rate on the RAR and GAR
(**a**) Following a stepwise stretch, tissue constructs exhibited both the RAR and GAR. (**b**) Following a slower stretch, the same tissue construct exhibited neither the RAR nor the very fast force shedding following the initial force rise (inset expands the time axis), but did exhibit the GAR. (**c**) Following an additional stepwise stretch on the same specimen, the RAR was recovered, indicating that the absence of the RAR in the second stretch was associated with the loading condition rather than permanent changes caused by the first stretch.